Smart Structures and Systems, *Vol. 29, No. 2 (2022) 287-299*
https://doi.org/10.12989/sss.2022.29.2.287

Post-earthquake fast building safety assessment using smartphone-based interstory drifts measurement

Ting Y. Hsu*[1,2,3], Cheng Y. Liu [1a], Yo M. Hsieh [1b] and Chi T. Weng [1c]

[1] *Department of Civil and Construction Engineering, National Taiwan University of Science and Technology, Taipei 10607, Taiwan*
[2] *Taiwan Building Technology Center, National Taiwan University of Science and Technology, Taipei 10607, Taiwan*
[3] *National Center for Research on Earthquake Engineering, Taipei 106219, Taiwan*

(*Received January 30, 2021, Revised September 12, 2021, Accepted October 18, 2021*)

Abstract. Rather than using smartphones as seismometers with designated locations and orientations, this study proposes to employ crowds' smartphones in buildings to perform fast safety assessment of buildings. The principal advantage of using crowds' smartphones is the potential to monitor the safety of millions of buildings without hardware costs, installation labor, and long-term maintenance. This study's goal is to measure the maximum interstory drift ratios during earthquake excitation using crowds' smartphones. Beacons inside the building are required to provide the location and relevant building information for the smartphones via Bluetooth. Wi-Fi Direct is employed between nearby smartphones to conduct peer-to-peer time synchronization and exchange the acceleration data measured. An algorithm to align the orientation between nearby smartphones is proposed, and the performance of the orientation alignment, interstory drift measurement, and damage level estimation are studied numerically. Finally, the proposed approach's performance is verified using large-scale shaking table tests of a scaled steel building. The results presented in this study illustrate the potential to use crowds' smartphones with the proposed approach to record building motions during earthquakes and use those data to estimate buildings' safety based on the interstory drift ratios measured.

Keywords: crowdsourcing; interstory drifts; orientation alignment; post-earthquake building safety; Wi-Fi Direct

1. Introduction

When a major earthquake strikes a large city, having prompt knowledge of many buildings' potential damage would be particularly useful to make timely decisions about the continuity of operations to improve earthquake resilience. Among many parameters, the interstory drift ratio (IDR) is accepted well as a reliable indicator for evaluating exceedance of selected limit states and the corresponding potential for building damage. Using the estimated maximum IDR and the application of various fragility curves provided in the technical manual of the earthquake model of the multi-hazard loss estimation methodology (FEMA 2013), assessments of buildings' post-earthquake damage can be conducted effectively and straightforwardly for different building types, heights, and seismic design levels. The application of measuring IDR to assess post-earthquake damage to 40 real buildings has been reported by Naeim *et al*. (2006).

Although many studies have been conducted on using a low-cost sensor network (Clayton *et al*. 2015, Finzi Neto *et al*. 2010, Kohler *et al*. 2016, Lei *et al*. 2020, Hsu *et al*. 2018), wireless sensor networks (Zonta *et al*. 2010, Haque *et al*. 2015, Sun *et al*. 2015, 2017, Kim *et al*. 2016a, b, Shen *et al*. 2021), and camera-based sensing networks (Dong *et al*. 2019, Yu *et al*. 2019, Hsu and Nieh 2020) to monitor structural health, it is still challenging to implement these networks widely because the total cost, including sensors, human labor, and system maintenance, is still high. On the other hand, much research has demonstrated smartphones' ability to measure accelerations in the 0.2-20 Hz frequency range and 5-2000 mg amplitude range (Dashti *et al*. 2014, Feng *et al*. 2015, Kong *et al*. 2016b). Yu *et al*. (2015) demonstrated that it is feasible to use smartphones to identify natural frequencies of cables on a cable-stay bridge. Ozer *et al*. (2015) showed that it is possible to identify a pedestrian link bridge's mode shapes using smartphones, provided the mode shapes obtained using synchronous data of high-quality accelerometers are available as a reference. Kong *et al*. (2018) illustrated the potential of using smartphones to record building shaking resulting from nearby earthquakes and using those data to extract the building's fundamental frequencies. Elhattab *et al*. (2019) showed that the difference in a bridge deck's operational frequencies (when normal traffic is passing) identified using smartphones and a wireless sensing network is approximately 1-3%. Shrestha *et al*. (2018) developed a bridge seismic monitoring system based on a smartphone

*Corresponding author, Associate Professor,
E-mail: tyhsu@ntust.edu.tw
[a] Master Student, E-mail: oulivedd@gmail.com
[b] Ph.D., Associate Professor,
E-mail: ymhsieh@ntust.edu.tw
[c] Research Assistant,
E-mail: m10305502@gapps.ntust.edu.tw

ISSN: 1738-1584 (Print), 1738-1991 (Online)

network using a cloud server to monitor a bridge long-term. The difference between the modal frequencies identified during earthquake events using the system developed and reference seismometers was 0.88% at maximum. Although these studies employed smartphones, they actually treated them as deployed sensor networks, in that the researchers designated the smartphones' locations and orientations. Besides, Mei and Gul (2018) proposed to use smartphones in a large number of moving vehicles as mobile sensors to detect damage of the bridges.

On the other hand, some researchers have attempted to employ smartphone-based crowdsourcing approaches for earthquake early warning purposes (Faulkner *et al*. 2014, Finazzi 2016, Kong *et al*. 2016a). When the smartphones are stable, e.g., resting on a desk or stand, this transforms them into portable seismometers that detect earthquakes. Further, Hsu and Nieh (2020) showed the possibility to use smartphones for on-site earthquake early warning after the trigger is classified as an earthquake event. This research has shown that using crowds' smartphones could allow for an earthquake's destructive effects to be reduced and prevented, and improve resilience. If numerous private smartphones distributed in buildings can be used to collect buildings' seismic vibration response, then it could overcome the substantial challenge of deploying a costly structural health monitoring (SHM) system in buildings, and provide a way to assess buildings' post-earthquake safety at very low cost in hardware and maintenance. However, to use private stable smartphones from crowds to estimate IDR, information on the smartphones' orientation and location is required, and the acceleration signals the different smartphones measure must be synchronized. In this study, we explore the use of crowds' smartphones to estimate IDR to assess post-earthquake building safety, and propose an algorithm to align the smartphones' orientation based on the vibration signals measured. Solutions to synchronize the smartphones and identify their location are also proposed. The methodology with which crowds' smartphones are used to measure IDR to estimate buildings' safety is explained in the next section. Next, the numerical study performed to verify the algorithm proposed to align nearby smartphones' orientation is described. After the experimental study of the proposed approach is presented, a discussion and conclusions are presented in the final section.

2. Methodology

In order to explain the procedures employed in using crowds' smartphones to perform post-earthquake building safety assessments, a flow chart of the procedures is shown in Fig. 1. The first two procedures have already been developed and utilized in earthquake early warning systems (Hsu and Nieh 2020); hence, only a brief introduction of the two procedures is provided here. In this study, we investigated whether crowds' smartphones in a stable state could be harnessed for IDR measurement using the smartphone application developed in this study. Note that only the smartphone lying horizontally will be treated as in a stable state. As stated above, to do so, information on the smartphones' orientation and location is required, and the acceleration signals different smartphones measure should be synchronized.

The first procedure in the overall process consists of detecting the occurrence of an earthquake event. To that end, the smartphones are triggered and de-triggered based on the short-term average/long-term average (STA/LTA) algorithm, which is often employed in geoscience research for earthquake event detection. The STA and LTA are the averages of the root mean square of three acceleration component signals of 20 and 500 points, respectively. When the smartphones remain de-triggered for more than 10 minutes, the state of the smartphones is defined as

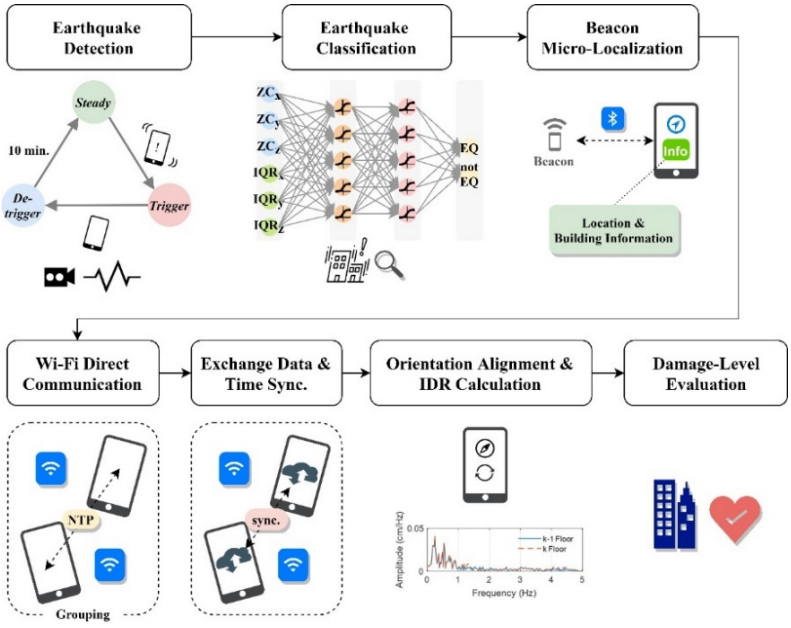

Fig. 1 The flow chart of the procedures using crowds' smartphones to perform post-earthquake building safety assessment

"Steady". To make sure the accelerations are measured only when the smartphones are lying horizontally, the state will not become "Steady" if the absolute value of the pitch or roll angles of the gyroscope in the smartphone is larger than 5°. Relatedly, only when the smartphones are triggered after having been in the "Steady" state will the triggering be viewed as indicative of a potential earthquake event, at which time the acceleration signals between the triggering and de-triggering of the event will be recorded. Hence, the mere vibrations of the smartphones carried by people will not be recorded.

The second procedure consists of distinguishing whether the recorded acceleration signals are due to an earthquake event or not. To that end, the artificial neural network (ANN) approach is employed to construct the earthquake classifiers. The ANN earthquake classifiers consist of one hidden layer of five neurons with sigmoid activation function and one output. The input features we used are the interquartile range (IQR) between the 25th and 75th percentile of the acceleration vector sum of the three-component acceleration and the zero-crossing (ZC) rate from the component with the highest value. High accuracy of classification can be achieved using the ANN approach, as indicated in Hsu and Nieh (2020).

If an event is classified as an earthquake event, the third procedure employed consists of obtaining the necessary building information and the smartphones' locations, which are provided by the pre-installed Bluetooth beacons in the building. Today, there are many interior products, e.g., light bulbs and smoke detectors (Cheng *et al*. 2017), that can be enhanced with Bluetooth beacons and form a Bluetooth mesh. These Bluetooth-beacon-equipped (BBE) products provide smartphone applications to help users find their location in a building and obtain necessary information about it. The typical price of a Bluetooth beacon device is only approximately 10 USD, and each Bluetooth beacon can cover an area of approximately 50 m in radius inside a building. In this study, we took advantage of the Bluetooth beacon to provide information about the beacon's location, structural type, number of stories, story height, and seismic design level for the smartphone application. The smartphone application can calculate IDRs using synchronized acceleration data collected by smartphones on adjacent floors and select the IDR thresholds using this building information based on the tables provided in the HAZUS-MH technical manual (FEMA 2013). In this study, we assume the smartphones are lying on a stiff furniture (nearly rigid body) and the out-of-plane deformation of the floor is neglecable (nearly shear building). Hence, when calculating the IDR, the height of the furniture where the smartphone are lying on is neglectable.

The fourth procedure consists of establishing a wireless connection between nearby smartphones using Wi-Fi Direct technology. This allows the phones to identify nearby peer devices and establish a direct wireless link without an intermediate Wi-Fi access point. Once the wireless link is established, two smartphones can communicate with each other at typical Wi-Fi speed; hence large-size acceleration data can be exchanged efficiently.

The fifth procedure consists of synchronizing the smartphones. Although each smartphone has a built-in clock, the time on the clock may not be sufficiently accurate because of drift if the smartphone does not update its clock from the Internet time servers regularly. Even with the regular and standard time synchronization mechanism referred to as NTP, smartphones may have hundreds and tens of milliseconds of error through early (Miškinis *et al*. 2011) and 5G (Borenius *et al*. 2019) mobile networks, respectively. We employed the NTP mechanism through Wi-Fi Direct link to synchronize the time of the acceleration signals recorded.

The sixth procedure consists of performing orientation alignment of the smartphones, after which the damage level of the building can be estimated by calculating the IDRs straightforwardly in the last procedure. Even with the above information ready, the smartphones' orientations are required to calculate the interstory drifts. Although most smartphones are equipped with a magnetometer, the orientation determined with it is not sufficiently accurate to calculate interstory drifts, particularly during the excitation of earthquakes. Kong *et al*. (2018) conducted forced-vibration tests on a nine-story building using a uniaxial shaker and measured the acceleration response using smartphones on the top floor. Because the vibration response was only along one direction, the orientation was estimated by rotating the signals measured until the energy of the acceleration time history on one of the horizontal components was minimized. However, this approach is not practical in real earthquake excitation cases where excitations occur in both directions.

In this study, we propose the least Fourier spectrum difference (LFSD) method to address orientation alignment in the frequency domain. Note that because only the smratphones lying steady and horiznotally will be used in this study, only the horiontal orientation (azimuth angle) is considered to be determined for orientation alignment. We assumed that the Fourier spectra of the acceleration data measured in the two horizontal components are distinct; hence, the pattern of the Fourier spectra will change as the smartphones' orientation changes. When the orientations of two smartphones on two adjacent floors are identical, the difference between their Fourier spectra $\Delta U_k(\omega_j, \theta)$ in both horizontal components, defined as Eq. (1), should be very small

$$\begin{aligned} \Delta U_k^x(\omega_j, \theta) &= \left| U_{k+1}^x(\omega_j, \theta) - U_k^x(\omega_j) \right| \\ \Delta U_k^y(\omega_j, \theta) &= \left| U_{k+1}^y(\omega_j, \theta) - U_k^y(\omega_j) \right| \end{aligned} \tag{1}$$

in which U_{k+1}^x represents the Fourier spectrum on the k+1 floor in the smartphone's local x-direction, and $\omega_j$represents the jth discrete frequency. The smartphone's orientation on the k+1th floor, θ, begins from the orientation of the smartphone on the kth floor. It will rotate at an interval of Δθ, and the rotated Fourier spectra of the k+1th floor are calculated as

$$\begin{aligned} U_{k+1}^x(\omega_j, \theta) &= U_{k+1}^x(\omega_j) \cos\theta + U_{k+1}^y(\omega_j) \sin\theta \\ U_{k+1}^y(\omega_j, \theta) &= -U_{k+1}^x(\omega_j) \sin\theta + U_{k+1}^y(\omega_j) \cos\theta \end{aligned} \tag{2}$$

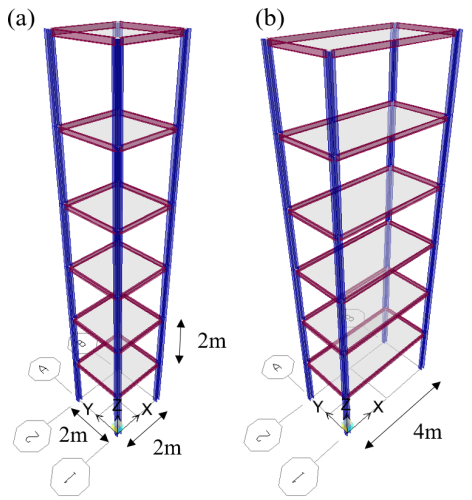

Fig. 2 The numerical model of the two six-story steel buildings: (a) building I; (b) building II

The summation of the Fourier spectra difference $\Delta U_k(\theta)$ is calculated as

$$\Delta U_k(\theta) = \sum_{j=1}^{M} \left(\Delta U_k^x(\omega_j, \theta) + \Delta U_k^y(\omega_j, \theta) \right) \quad (3)$$

in which M represents the total number of discrete frequencies considered. The orientation with the smallest value of $\Delta U_k(\theta)$ was selected as the best estimation of the orientation, denoted as θ_B. As a result, the interstory drifts in both horizontal directions between the k^{th} and $k+1^{th}$ floor were calculated using the orientation selected. The maximum value of the Euclidean norm of the interstory drifts in both horizontal directions during an earthquake excitation were calculated and used to determine the damage level of the story.

3. Numerical study of the LFSD method

To understand the proposed LFSD method's potential performance, the linear elastic earthquake response of two six-story steel buildings with a 2% damping ratio excited during 21 earthquakes simulated using the ETABS commercial software was studied, as shown in Fig. 2. The dimensions of each story of building I were 2.0 m wide × 2.0 m deep × 2.0 m high, while those of building II were 4.0 m wide × 2.0 m deep × 2.0 m high. The additional mass of each floor was approximately 388.1 kg/m^2, and the total mass of buildings I and II was 15194 and 24509 kg, respectively. Each beam and column were made of A572Gr50 steel and had an H-shaped cross-section of 125 × 60 × 6 × 8 mm and 150 × 150 × 7 × 10 mm, respectively. The column's weak axis was along the global X-direction of the building. The fundamental natural frequencies of building I in the X and Y directions were 1.33 and 1.14 Hz, and those of building II were 0.77 and 0.86 Hz, respectively. The 21 earthquakes were collected from the Significant Earthquakes provided by the United States

Table 1 The 21 earthquakes considered in the numerical study

Earthquake	*Region*	*Station*	*Date*	*M*	*PGA*
El Centro	US/CA	USGS station 0117	1940/05/19	6.9	342
Taft	US/CA	USGS station 1095	1952/07/21	7.5	176
India-Burma Border	India	IITR station berl	1988/08/06	7.2	337
Loma Prieta (Cptl.)	US/CA	CSMIP station 47125	1989/10/18	7.0	463
Loma Prieta (Corra.)	US/CA	CSMIP station 57007	1989/10/18	7.0	618
Northridge (Van)	US/CA	CSMIP station 24386	1994/01/17	6.7	445
Northridge (Newhall)	US/CA	CSMIP station 24279	1994/01/17	6.7	578
Northridge (Tarzana)	US/CA	CSMIP station 24436	1994/01/17	6.7	1745
Kobe	Japan	CUE station	1995/01/16	6.9	500
Northwest China	China	CSB station 19001	1997/04/11	6.1	294
Chi Chi	Taiwan	TCU084	1999/09/21	7.6	985
Hector Mine	US/CA	USGS station 5075	1999/10/16	7.1	59
Lefkada	Greece	Lefkada No1	2003/08/14	6.3	417
Wenchuan	China	051WCW	2008/05/12	8.0	958
Samoa Islands	Samoa	Afiamalu	2009/09/29	8.0	93
Miyagi	Japan	MYG012	2011/04/07	7.1	1447
Central Italy	Italy	Forca Canapine	2016/10/30	6.6	910
Valparaiso	Chile	Torpederas	2017/04/24	6.9	889
Puebla	Mexico	UNAM	2017/09/19	7.1	54
Hualien	Taiwan	ENA	2018/02/06	6.2	428
Anchorage	US/CA	Rabbit Creek	2018/11/30	7.0	652

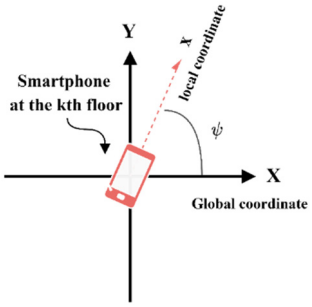

Fig. 3 The definition of the orientation of the crowds' smartphones on the k[th] floor

(a)

Level	IDR
N	0% ~ 0.4%
S	0.4% ~ 0.8%
M	0.8% ~ 2%
E	2% ~ 5.33%
C	≧ 5.33%

(b)

Estimate \ Actual (%)	N	S	M	E	C
N	23.0	0	0	0	0
S	0	12.3	0	0	0
M	0	0	39.5	0.2	0
E	0	0	0.2	24.8	0
C	0	0	0	0	0

Fig. 4 (a) The IDR thresholds of each damage level based on the tables provided in the HAZUS-MH technical manual; (b) The typical normalized confusion matrix. N, S, M, E, and C represent No, Slight, Moderate, Extensive, and Complete damage levels, respectively

Geological Survey (USGS) and the Consortium of Organizations for Strong Motion Observation Systems (COSMOS), as well as the strong earthquakes provided by the Taiwan Strong Motion Instrumentation Program (TSMIP), as listed in Table 1.

Because the orientation of the crowds' smartphones on the k[th] floor should be arbitrary, and the results of the orientation alignment determined by the proposed LSFD method could also differ at different orientations, the orientation of the smartphones on the k[th] floor was also considered in this study. The orientation of the crowds' smartphones on the k[th] floor was defined as Ψ, as shown in Fig. 3.

The original data the crowds' smartphones measured were actually the absolute acceleration structural response during the earthquakes. Complex values of the Fourier spectrogram of the absolute acceleration structural response were obtained after the fast Fourier transform, and often only the amplitude of the Fourier spectrogram was used. In this study, we proposed to use the complex value of the Fourier spectrogram of the absolute displacement structural response during the earthquakes with the LSFD method to align the orientation of the crowds' smartphones between adjacent floors. The displacement data were obtained after double integration of the acceleration data and a fourth-order high-pass Butterworth filter with a cut-frequency of 0.2 Hz.

In the following numerical studies, for each floor, 360 orientations of Ψ between 0° and 359° with an interval of 1°, i.e., ΔΨ, were considered. The general performance of all six floors, 21 earthquakes, and 360 orientations of each floor of the two building models, e.g., 90720 cases in total, was calculated. For each case, the best orientation was determined using a scanning process. In this process, 360 orientations of between 0 and 359 with $\Delta\theta$=1° were calculated, and that with the smallest value of $\Delta U_k(\theta)$ was selected as the best orientation. Then, using those best orientations, the drift ratios of each case were calculated. Based on the IDR calculated, the damage level was estimated based on the tables provided in the HAZUS-MH technical manual (FEMA 2013), as summarized in Fig. 4(a), with the typical confusion matrix of damage levels shown in Fig. 4(b). The accuracy of the estimated damage levels based on the confusion matrix was also calculated by summing the diagonal components of the normalized confusion matrix.

Firstly, we compared the results of the LSFD using the proposed complex value of the displacement spectrogram (denoted as Type II) to those using only the amplitude of the same spectrogram (denoted as Type I). The typical complex value of the displacement spectrogram and the amplitude of the same spectrogram are shown in Fig. 5. In this typical case, the length of acceleration time history is 2048 with 50 Hz, hence the measurement duration is 2048/50 = 40.96 s. The frequency interval of this Fourier spectrogram is 0.0244 Hz. Because both real and imaginary parts are employed, more information is used for the orientation

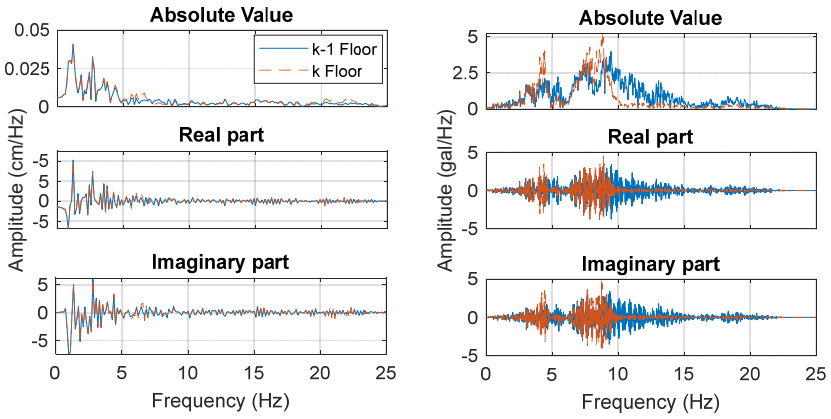

Fig. 5 Typical amplitude and complex Fourier spectrograms of displacement (left) and acceleration (right)

Table 2 Comparison of the LSFD method's performance using the proposed complex value of the displacement spectrogram (Type II) and that using only the amplitude of the same spectrogram (Type I)

Type	θ (°)		IDR (%)			Damage level
	RMSE	Max. $\lvert E_\theta \rvert$	RMSE	Max. E_{IDR}	Min. E_{IDR}	Accuracy (%)
I	1.35	11	0.039	0.426	-0.178	99.0
II	0.60	4	0.015	0.111	-0.101	99.6

Table 3 Comparison of LSFD method's performance using the proposed complex value of the displacement spectrogram and that using the acceleration spectrogram

Response	θ (°)		IDR (%)			Damage level
	RMSE	Max. $\lvert E_\theta \rvert$	RMSE	Max. E_{IDR}	Min. E_{IDR}	Accuracy (%)
Disp.	0.60	4	0.015	0.111	-0.101	99.6
Disp. (0-10 Hz)	0.60	4	0.015	0.111	-0.101	99.6
Acc.	45.21	180	1.159	16.464	-0.228	90.5
Acc. (0-10 Hz)	27.24	180	1.090	16.464	-0.228	95.2

alignment than for the alignment for which only the amplitude is used. The root-mean-square error (RMSE) of the best orientations using the proposed complex value of displacement spectrogram was 0.60°, and the maximum absolute error was 4.0°. On the other hand, the RMSE of the best orientations using the amplitude of the same spectrogram was 1.35°, and the maximum absolute error was 11.0°. The RMSEs and ranges of the IDRs' errors, as well as the estimated damage levels' accuracy, are also summarized in Table 2. Both the RMSEs of the Type I and II IDRs were quite small, less than 0.04%, and both of the accuracies were quite large, equal to or greater than 99.0%. Apparently, Type II outperformed Type I, because all of the error indices in the table were smaller and the accuracy index was higher. As a result, only Type II was employed in the following studies.

Next, we compared the results of the LSFD using the proposed complex value of the displacement spectrogram to those using the acceleration spectrogram. The RMSEs and ranges of both the best orientations and the IDRs, as well as the estimated damage levels' accuracy, are summarized in Table 3. Clearly, using displacement was much better than using acceleration to align the orientation in this study. Observing the typical displacement and acceleration Fourier spectrograms of adjacent floors in Fig. 5, it can be seen that their displacement spectrograms were very similar, whereas the acceleration spectrograms were quite different, which made it difficult to align the orientation using acceleration

Table 4 The LSFD method's performance for different stories using the truncated displacement spectrograms

Story	θ (°)		IDR (%)			Damage level
	RMSE	Max. $\lvert E_\theta \rvert$	RMSE	Max. E_{IDR}	Min. E_{IDR}	Accuracy (%)
1S	0.34	1	0.007	0.053	-0.027	100.0
2S	0.74	4	0.014	0.077	-0.053	98.6
3S	0.80	4	0.018	0.111	-0.055	100.0
4S	0.69	4	0.017	0.107	-0.048	100.0
5S	0.55	2	0.017	0.099	-0.088	98.9
6S	0.35	2	0.011	0.081	-0.101	100.0

data. Because most of the fundamental natural frequencies of typical buildings are smaller than 10 Hz, the results using only the frequency range below 10 Hz were also calculated and are shown in Table 3. The results when the acceleration data were used improved somewhat, but still were much worse than those using displacement data. Further, as the results of using displacement data with a frequency range below 10 Hz were identical to those using the full frequency range because the spectrograms in the high frequency range contributed little (as shown in Fig. 5), we used only the truncated displacement spectrograms in the following studies to reduce the computational effort.

We evaluated the performance of aligning the orientation of different stories using the truncated displacement spectrograms as well, and the results are summarized in Table 4. We observed that the general performance in the middle stories was slightly worse than that in the low and high stories. This was probably because the absolute displacement measured consisted of both ground excitation and the structural relative response, as illustrated in Fig. 6. The absolute displacement data on the adjacent floors of the low and high stories were more likely dominated by the ground excitation and structural relative response, respectively, while those of the middle stories were not, but were more likely a mix of both the ground excitation and structural relative response.

The noise in the displacement data measured may affect the results of orientation alignment. The standard deviation of noise signals, i.e., noise floor, of the typical smartphones used in the previous study was approximately 2.0 cm/s^2 (gal) at maximum (Hsu and Nieh 2020), and that of those used in this study was approximately 0.6 cm/s^2 on average (as described later in the section on the experimental study). Hence, noise floors of 0.5, 2.0, and even 3.5 cm/s^2 were added to the acceleration data, and then the orientation alignment was performed using the truncated displacement spectrograms. The results are summarized in Table 5. In the results with the 0.5 cm/s^2 noise floor, the accuracy of the damage level estimations was very high, i.e., 99.18%. Even in the results with the 3.5 cm/s^2 noise floor, the damage level estimations' accuracy was still very promising, i.e., 95.51%.

In the results above, the best orientations were obtained

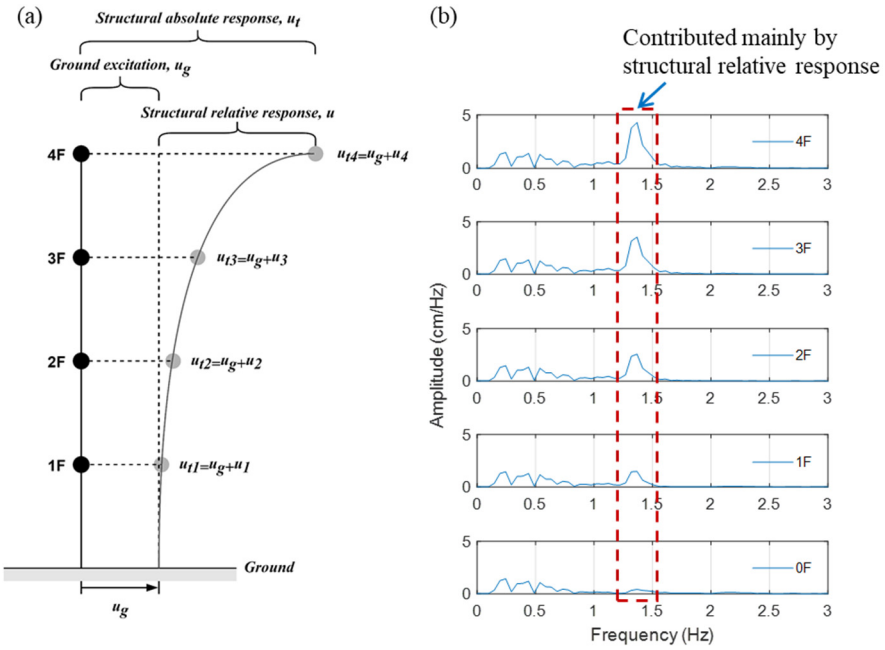

Fig. 6 Schematic diagram showing (a) the absolute displacement measured, which consisted of both ground excitation and the structural relative response, and (b) the displacement Fourier spectrograms of each floor

Table 5 The LSFD method's performance under different noise levels using the truncated displacement spectrograms

Noise (gal)	θ (°)		IDR (%)			Damage level
	RMSE	Max. $\lvert E_\theta \rvert$	RMSE	Max. E_{IDR}	Min. E_{IDR}	Accuracy (%)
0.5	0.79	5	0.018	0.116	-0.092	99.18
2	1.04	5	0.036	0.144	-0.118	97.07
3.5	1.43	8	0.066	0.276	-0.180	95.51

Table 6 The LSFD method's performance using different in the scanning process

Δθ (°)	θ (°)		IDR (%)			Damage level
	RMSE	Max. $\lvert E_\theta \rvert$	RMSE	Max. E_{IDR}	Min. E_{IDR}	Accuracy (%)
0.1	0.57	3.9	0.0136	0.0944	-0.0754	99.09
0.3	0.58	4.0	0.0138	0.1035	-0.0797	99.17
0.5	0.59	4.1	0.0141	0.1129	-0.0839	99.19
0.7	0.61	4.2	0.0146	0.1225	-0.0925	99.20
1	0.64	4.3	0.0156	0.1374	-0.1015	99.17
2	0.82	4.7	0.0208	0.2135	-0.1431	98.98
3	1.06	5.2	0.0277	0.3295	-0.1844	98.68

by the scanning process with $\Delta\theta = 1°$. If a smaller $\Delta\theta$ was used, we anticipated that better results could be achieved because a smaller error in the best orientations could be obtained. Hence, the effects of using different $\Delta\theta$ were

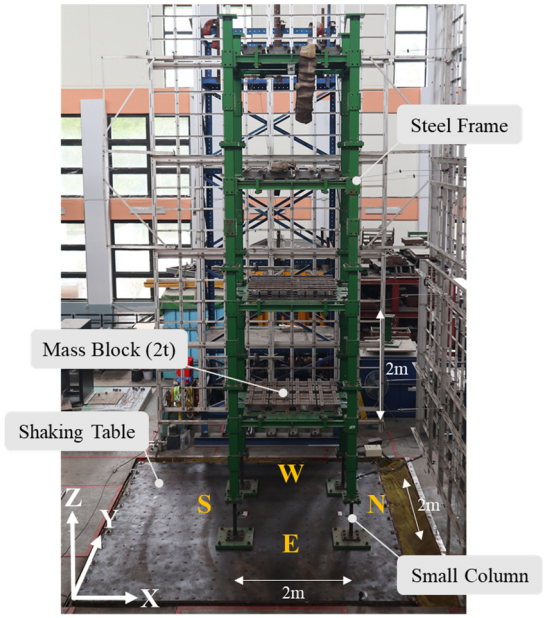

Fig. 7 The scaled, four-story steel building structure on a shaking table

studied herein. The $\Delta\theta$ considered were 0.1°, 0.3°, 0.5°, 0.7°, 1°, 2°, and 3°. Because smaller Δθ s were used, smaller Δψ s of 0.1° were also employed accordingly. The results using different $\Delta\theta$ are summarized in Table 6. Although smaller errors were obtained for both the estimated best orientation and IDR, the improvement in the errors decreased when $\Delta\theta$ was smaller than 1°. In addition, the accuracy of the damage level estimation appeared to become saturated when $\Delta\theta$ decreased to 1°. Therefore, $\Delta\theta = 1°$ was recommended for practical application to save computational effort in crowds' smartphones.

Table 7 The 14 earthquakes induced in the shaking table tests

No.	Earthquakes	Station	Axial	Scale	PGA (cm/s^2)
1	Hualien	HWA048	XYZ	10%	36
2	Meinong	CHY061	XYZ	10%	28
3	Chi Chi	TCU089	XYZ	10%	35
4	El Centro	USGS station 0117	XYZ	10%	46
5	Kobe	JMA station	XYZ	10%	99
6	Hualien	HWA048	XYZ	20%	72
7	Meinong	CHY061	XYZ	20%	56
8	Chi Chi	TCU089	XYZ	20%	69
9	El Centro	USGS station 0117	XYZ	20%	91
10	Kobe	JMA station	XYZ	20%	199
11	Hualien	HWA048	XYZ	30%	108
12	Meinong	CHY061	XYZ	30%	84
13	Chi Chi	TCU089	XYZ	30%	104
14	El Centro	USGS station 0117	XYZ	30%	137

4. Experimental study

A scaled, four-story steel building structure designed and constructed at the National Center for Research on Earthquake Engineering (NCREE) in Taiwan was used to test the proposed post-earthquake building safety assessment using crowds' smartphones experimentally, as shown in Fig. 7. Each story's dimensions and mass, as well as the structural elements' size were identical to those of the building used in the numerical study. There were six stories in the steel building structure in the initial tests. However, a severe rocking interaction between the shaking table and the structure was observed, even during small excitations. To allow the structural responses to cover a larger range of IDRs and avoid the rocking interaction simultaneously, the number of stories was reduced to four, and the dimension of the bottom of the columns on the first story was reduced to $150 \times 50 \times 7 \times 10$ mm. The fundamental natural frequencies were 1.17 and 1.88 Hz along the X- and Y-directions, respectively.

Five different earthquakes with scales of 10%, 20%, and 30% were used to excite the structure, except the Kobe earthquake because of safety consideration. The 20% Kobe earthquake had already induced a large nonlinear interstory drift and the larger 30% Kobe earthquake may have caused the structure to collapse. In total, 14 earthquakes were excited during the shaking table tests, and their PGA was between 28 to 199 cm/s^2, as shown in Table 7.

Five Sharp Aquos V smartphones were mounted on the north side of each floor, while Sharp Aquos Zero, Oppo A5 2020, Sharp Aquos V, RealMe 5, and Xiaomi Mi A3 were mounted on the ground floor (0F), 1F, 2F, 3F, and 4F on the south side, respectively. These smartphones' noise floor and the resolution of the acceleration measurement were approximately 0.6 and 0.3 cm/s^2, respectively, as shown in Table 8. The smartphones' orientation on the 0F, 1F, 2F, 3F, and 4F was 0°, 30°, 60°, 90°, and 120°, respectively. The typical arrangement of the orientation of the smartphone on the 4F is shown in Fig. 8(a). Because specific orientation of the smartphone on each floor during the experimental tests is demanded, in order to have the orientation of the smartphone accurately placed, a transparent acrylic plate marked with datum lines was attached on the floor via double-sided tape. Hence the smartphone is also attached on

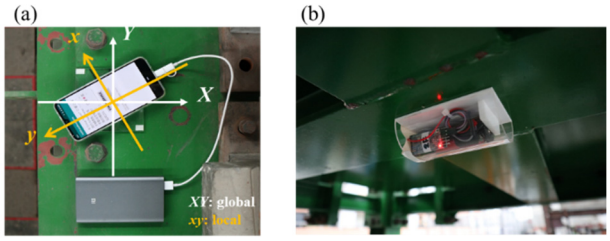

Fig. 8 (a) The typical arrangement of the orientation of the smartphone on the 4F; and (b) the typical Bluetooth low energy beacon mounted under the floor

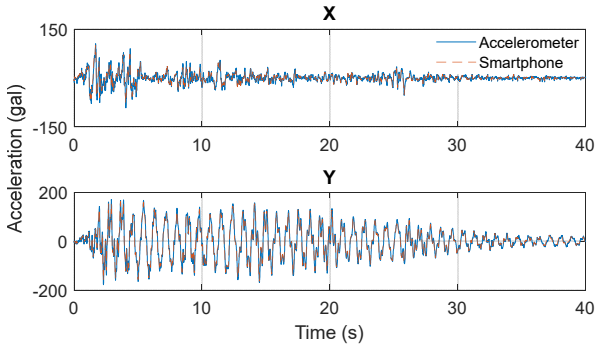

Fig. 9 The typical accelerations measured by the smartphones and the accelerometers in the X- (uppper) and Y- (lower) directions

Table 8 The smartphones used in the experimental study

Vendor	Model	Accelerometer type	Noise floor (cm/s^2)	Resolution (cm/s^2)	Release
Xiaomi	Mi A3	BMI160 Accelerometer	0.899	0.239	2019
OPPO	A5 2020	LSM6DS3C Accelerometer	0.468	0.120	2019
RealMe	realme 5	ICM4x6xx Accelerometer	0.390	0.479	2019
SHARP	AQUOS V	ICM40605 Accelerometer	0.576	0.119	2019
SHARP	AQUOS zero	LSM6DSM Accelerometer	0.708	0.478	2019
		Average	0.608	0.287	

Table 9 The smartphones used in the experimental study

Story No.	Maximum acceleration (cm/s^2)		Maximum IDR (%)	
	Northside	Southside	Northside	Southside
4	451	421	0.397	0.352
3	376	364	0.720	0.795
2	313	293	0.835	0.866
1	197	196	1.467	1.500

the acrylic plate via double-sided tape to prevent sliding on the smooth surface of the acrylic plate. The measured accelerations from the smartphones were very close to the ones measured by the accelerometers. An example of the typical accelerations measured by the smartphones and the accelerometers is shown in Fig. 9. During the tests, the smartphones on the north side were connected to each other using Wi-Fi Direct, as were those on the south side. Thus, the IDRs were calculated on the north and south sides separately using the smartphones on each story. The measured maximum acceleration response and the maximum IDR of each story of a typical earthquake excitation are summarized in Table 9. Although the maximum acceleration response of lower stories was smaller, the IDR of lower stories was much larger, especially the first story.

In addition to the smartphones, three LVDTs and three accelerometers were installed on each floor of the building specimen, as shown in Fig. 10. The LVDTs and accelerometers' signals were digitized at 200 Hz, while the smartphones' sampling rate was 50 Hz. Five Bluetooth low energy beacons based on Texas Instruments CC2541 were mounted under/on the floors; a typical one is shown in Fig. 8(b). The smartphones can detect the Bluetooth signals of several nearby beacons, and the beacon with the largest Received Signal Strength Indicator (RSSI) was selected automatically and information on the story height and location were then provided by the beacon that was selected.

The smartphones triggered when Eq. (4) was satisfied for 0.2 s continuously, and de-triggered when Eq. (5) was satisfied for 1 s. The threshold in the equations was defined as the average value of the STA (μ_{STA}) plus four times the standard deviation of the STA (σ_{STA}) when the smartphones remained steady on the structure for 1 minute, as calculated using Eq. (6)

$$STA > 2LTA \text{ or } STA > threshold \tag{4}$$

$$STA < LTA_{trigger} \text{ and } STA < threshold \tag{5}$$

$$threshold = \mu_{STA} + 4\sigma_{STA} \tag{6}$$

Because there was high hydraulic pressure in the actuators under the shaking table, some background vibration was induced even without earthquake excitation. The background vibration's noise floor was very high, approximately 5.0 cm/s^2. Such a large background vibration is not normal in real application, and made it difficult to trigger and de-trigger the earthquakes during the tests, particularly for the small earthquakes. Among the 112 cases (14 earthquake excitations × 4 stories × 2 sides), only 106 cases were valid because 6 cases were not triggered successfully on the low stories during some of the earthquake excitations with a 10% scale because of the

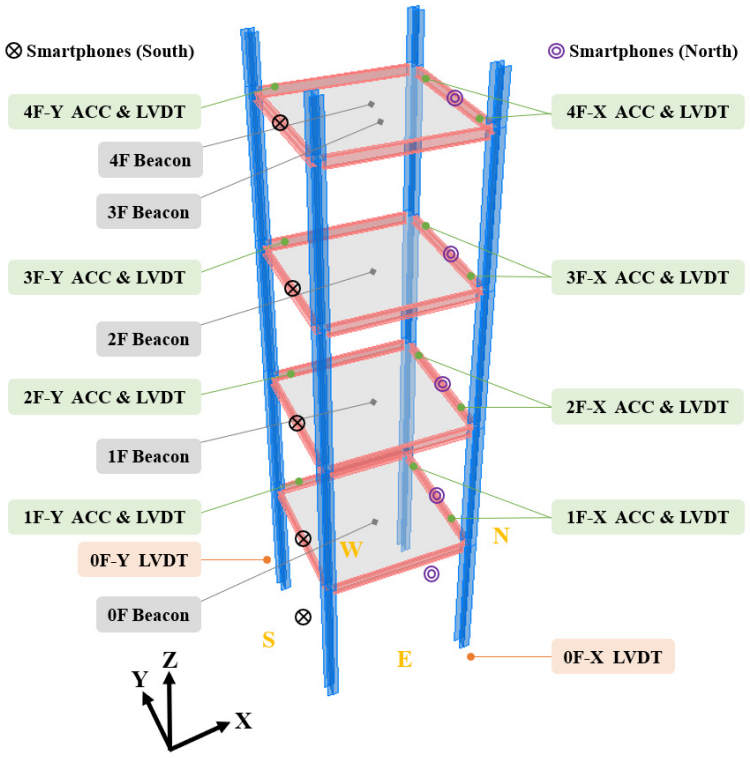

Fig. 10 The locations of the smartphones, LVDTs, and accelerometers installed on each floor of the building specimen

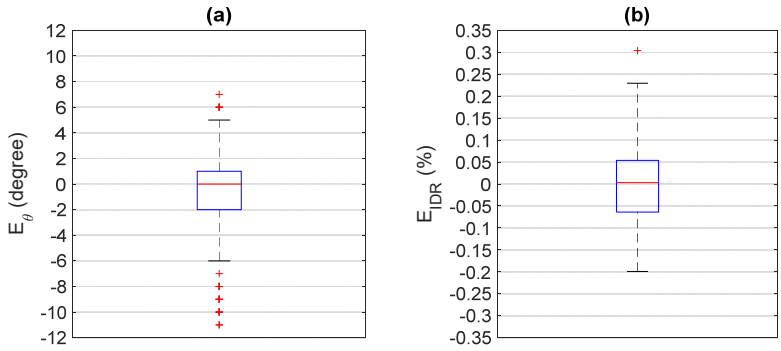

Fig. 11 Boxplot of (a) E_θ; and (b) E_{IDR} in the experimental study

large noise floor.

Because the noise floor of the smartphones used in this study is approximately 0.6 gal, if the smartphones have difficulty to trigger and de-trigger during earthquake excitations in practical applications, the maximum acceleration of these small earthquakes is anticipated to be approximately only several gals. Hence these small earthquakes are not possible to damage the buildings. In other words, safety assessment is not required to be conducted after these small earthquakes and no acceleration records are required to be collected from the smartphones.

In addition, due to the large background vibration, the function of earthquake classification was disabled during the experimental tests. The performance of the earthquake classification has been verified through experimental tests using an electric shake table system (Hsu and Nieh 2020).

Before the earthquake tests, the performance of synchronizing the smartphones' time using the NTP mechanism was studied. The smartphones were mounted on the shaking table and the table was excited using white noise with PGA of approximately 30 cm/s^2. The time delay Δt_k at frequency ω_k was estimated based on the phase difference $\Delta\phi_k$ using the following equation

$$\Delta t_k = \Delta\phi_k \cdot \frac{\omega_k}{2\pi} \tag{7}$$

The estimated time delay between each pair of smartphones was only 0.00458 s on average within the frequency range of 0.1 to 25 Hz, which was approximately one-fourth of the sampling interval of 0.02 s. Although the performance of synchronizing the time using the NTP mechanism was not perfect, it appears to be acceptable to estimate the IDR using the smartphones, as can be observed in the following results.

The performance of the proposed approach in the 106 cases during the earthquake excitations was studied herein. Because the actual orientation of the smartphones on each floor was known, the errors in their estimated orientations, denoted as E_θ, using the proposed orientation alignment approach, i.e., the LFSD method, were calculated. The boxplot of E_θ is shown in Fig. 11(a), which indicates that more than half of the E_θ were between ±2°, and some of the outliers reached 9° and -11°. The RMSE of E_θ was 4.260.

The procedure to calculate the IDR in the experimental

Smartphone \ LVDT	N	S	M	E	C
N	64	1	0	0	0
S	4	25	0	0	0
M	0	2	14	2	0
E	0	0	0	0	0
C	0	0	0	0	0

Fig. 12 The confusion matrix of the estimated damage levels in the experimental study

tests is summarized hererin. After the earthquake excitations, the acceleration data between trigger and de-trigger were recorded. The time delay between two adjacent floors were calculated based on the NTP mechanism and then time synchronizing was performed accordingly. The intersection of the synchronized acceleration between two adjacent floors were used and then double integrations and high-pass filter were conducted to obtain displacement time histories. The fast Fourier transform of length 2^N was conducted to obtain Fourier spectragrams and then the LSFD method was performed for orientation alignment. Zero padding was added to the displacement time histories to achieve the smallest number of N so that length 2^N was larger than the length of the original displacement time histories. Hence the length 2^N was determined based on the length of the displacement time histories and could be different for each pair of adjacent displacement time histories during different earthquake excitations. Finally, the IDRs was calculated using the displacement time histories and the story height provided by the beacons after orientation alignment.

The interstory drifts during the earthquakes can be calculated using the LVDT, and the maximum drifts the LVDT measured were used as the reference. The error of the maximum IDRs, denoted as E_{IDR}, of the 106 cases during the earthquake excitations was calculated, and the boxplot of the E_{IDR} is shown in Fig. 11(b). Approximately half of the E_{IDR} were between ±0.05%, and some of the outliers reached approximately 0.3% and -0.2%. The RMSE of E_{IDR} was 0.091%.

With respect to the estimated damage levels of the 106

Table 10 The performance of the proposed approach during different earthquake excitations (from small to large IDR)

Earthquake	Max. IDR (%)	RMSE		Damage level
		θ (degree)	IDR (%)	Accuracy (%)
10%CHY061	0.150	4.30	0.050	100.0
20%CHY061	0.260	2.18	0.040	100.0
10%HWA048	0.280	4.05	0.077	100.0
10%TCU089	0.311	4.66	0.079	100.0
30%CHY061	0.353	2.81	0.045	100.0
20%HWA048	0.535	4.00	0.071	100.0
10%El Centro	0.548	5.58	0.093	87.5
20%TCU089	0.653	4.54	0.087	87.5
30%HWA048	0.779	2.94	0.126	87.5
30%TCU089	0.988	3.55	0.088	87.5
10%Kobe	1.062	5.71	0.160	75.0
20%El Centro	1.071	4.99	0.050	100.0
30%El Centro	1.500	4.89	0.097	87.5
20%Kobe	2.140	3.76	0.129	75.0

cases during the earthquake excitations, the confusion matrix is shown in Fig. 12. Two cases in which the damage level was extensive were under-estimated, as the confusion matrix showed a moderate damage level. It was confirmed that, even if the orientation alignment was perfect, the damage levels in these two cases—the smartphones on the north and south sides of the first story during the 20% Kobe earthquake—were still under-estimated. The maximum IDR the LVDT measured was 2.14%, while those the smartphones measured were 1.96%, an under-estimate of approximately 0.17%. One of the reasons for these errors could be that the high-pass filter filtered out the nonlinear low-frequency drifts content after double integration of the acceleration signals. Other reasons could be errors in synchronizing the time and the discrete measurement using different sampling rates between the smartphones and LVDTs. Nevertheless, the damage level estimation's accuracy was 92.0%, which supported the feasibility of the proposed approach.

In order to observe the performance of the proposed approach during different amplitudes of earthquake excitations, the RMSEs of the estimated orientations and IDR and the damage level estimation's accuracy are summarized in Table 10. Whereas the amplitude of earthquake excitations seems to affect the RMSEs of the estimated orientations only a little, it seems that the RMSEs of the estimated IDR increased and the damage level estimation's accuracy decreased as the amplitude of the earthquake excitations increased. These results imply that some nonlinear response could occur during larger earthquake excitations, and that some of these signals could be filtered out and hence induce larger errors of IDR estimation.

In general, the errors in the smartphones' orientations was much larger than those in the numerical study, which could be caused primarily by the extraordinarily large background excitation. As a result, the performance of the interstory drifts measurement and damage level estimation was affected.

5. Conclusions

This study proposed to use crowds' smartphones distributed in a building to estimate a building's damage level during earthquake excitation based on the estimated maximum IDRs. Originally, the information on the smartphones' orientation and location was not known, and the acceleration signals different smartphones measured were not synchronized. In this study, the LSFD method was proposed to align the smartphones' orientation based on the vibration signals measured. The nearby beacons broadcasted using Bluetooth provided the location and relevant building information. The Wi-Fi Direct was employed to identify and connect the nearby smartphones and exchange data between them; hence, the smartphones could be synchronized based on the NTP mechanism and their orientation aligned using the proposed LSFD method. As a result, the IDRs of each story of the building could be calculated based on the absolute acceleration response the smartphones on each floor of the building measured during the earthquake excitations, and the damage level of each story of the building could be estimated based on preassigned thresholds of the IDRs.

The proposed LSFD method's performance was studied using the numerical model of a steel building under different earthquake excitations. Based on the results of the numerical study, the complex value of the Fourier spectra of the displacement response signals was preferred for the LSFD method, rather than the absolute value of the Fourier spectra of the acceleration response signals. The damage level estimations' accuracy is very promising given the noise level of the smartphones considered during the simulated earthquakes. When performing the scanning process with the LSFD method to determine the best orientation, the scanning interval $\Delta\theta=1°$was recommended for practical application to save computational effort in the crowds' smartphones. Further, because most of the fundamental natural frequencies of typical buildings are smaller than 10 Hz, it is also suggested to use only the frequency range below 10 Hz to reduce computational effort.

The necessary algorithms were embedded in the smartphone applications, and the proposed approach was verified using shaking table tests of a scaled, four-story steel building. The time difference between the smartphones when they were synchronized using the NTP algorithm via Wi-Fi Direct was 0.00458s on average, approximately one-quarter of the acceleration records' sampling interval, i.e., 0.02 s. Although the error in the estimated best orientation during the experimental tests in the presence of extraordinarily large background excitation could reach 11° at maximum, the RMSE of the E_{IDR} was smaller than 0.1%. As a result, the accuracy of the damage level estimation can reach 92%. Thus, the numerical and

experimental results illustrate the potential of using crowds' smartphones to evaluate buildings' post-earthquake safety using the proposed approach. Since large earthquakes do not often occur, in order to validate the proposed approach, it may be necessary to conduct an experiment in a tall building during typhoon season in the future.

Acknowledgments

The authors want to thank the National Center for Research on Earthquake and Engineering, Taiwan for their support. This work was also financially supported by the Taiwan Building Technology Center from The Featured Areas Research Center Program within the framework of the Higher Education Sprout Project by the Ministry of Education in Taiwan.

References

Borenius, S., Costa-Requena, J., Lehtonen, M. and Kantola, R. (2019), "Providing Network Time Protocol Based Timing for Smart Grid Measurement and Control Devices in 5G Networks", *Proceedings of 2019 IEEE International Conference on Communications*, *Control*, *and Computing Technologies for Smart Grids* (*SmartGridComm*), Beijing, China, pp. 1-6.

Cheng, M.Y., Chiu, K.C., Hsieh, Y.M., Yang, I.T., Chou, J.S. and Wu, Y.W. (2017), "BIM integrated smart monitoring technique for building fire prevention and disaster relief", *Automat. Constr.*, **84**, 14-30. https://doi.org/10.1016/j.autcon.2017.08.027

Clayton, R.W., Heaton, T., Kohler, M., Chandy, M., Guy, R. and Bunn, J. (2015), "Community seismic network: A dense array to sense earthquake strong motion", *Seismol. Res. Lett.*, **86**(5), 1354-1363. https://doi.org/10.1785/0220150094

Dashti, S., Bray, J.D., Reilly, J., Glaser, S., Bayen, A. and Mari, E. (2014), "Evaluating the reliability of phones as seismic monitoring instruments", *Earthq. Spectra*, **30**(2), 721-742. https://doi.org/10.1193/091711EQS229M

Dong, C.Z., Bas, S. and Catbas, F.N. (2019), "A completely non-contact recognition system for bridge unit influence line using portable cameras and computer vision", *Smart Struct. Syst.*, *Int. J.*, **24**(5), 617-630. https://doi.org/10.12989/sss.2019.24.5.617

Elhattab, A., Uddin, N. and Obrien, E. (2019), "Extraction of bridge fundamental frequencies utilizing a smartphone MEMS accelerometer", *Sensors*, **19**, 3143. https://doi.org/10.3390/s19143143

Faulkner, M., Clayton, R., Heaton, T., Chandy, K.M., Kohler, M., Bunn, J., Guy, R., Liu, A., Olson, M., Cheng, M.H. and Krause, A. (2014), "Community sense and response systems: Your phone as quake detector", *Commun. ACM*, **57**, 66-75. https://doi.org/10.1145/2622633

Federal Emergency Management Agency, (2013), HAZUS-MH2.1 Technical Manual, Washington, DC, USA.

Feng, M., Fukuda, Y., Mizuta, M. and Ozer, E. (2015), "Citizen Sensors for SHM: Use of accelerometer data from smartphones", *Sensors*, **15**, 2980-2998. https://doi.org/10.3390/s150202980

Finazzi, F. (2016), "The earthquake network project: Toward a crowdsourced smartphone-based earthquake early warning system", *Bull. Seismol. Soc. Am.*, **106**, 1088. https://doi.org/10.1785/0120150354

Finzi Neto, R.M., Steffen Jr, V., Rade, D.A., Gallo, C.A. and Palomino, L.V. (2010), "A low-cost electromechanical impedance-based SHM architecture for multiplexed piezoceramic actuators", *Struct. Health Monit.*, **10**, 391-402. https://doi.org/10.1177/1475921710379518

Haque, M.E., Zain, M.F.M., Hannan, M.A. and Rahman, M.H. (2015), "Building structural health monitoring using dense and sparse topology wireless sensor network", *Smart Struct. Syst., Int. J.*, **16**(4), 607-621. https://doi.org/10.12989/sss.2015.16.4.607

Hsu, T.Y. and Nieh, C.P. (2020), "On-site earthquake early warning using smartphones", *Sensors*, **20**, 2928. https://doi.org/10.3390/s20102928

Hsu, T.Y., Yin, R.C. and Wu, Y.M. (2018), "Evaluating post-earthquake building safety using economical MEMS seismometers", *Sensors*, **18**(5), 1437. https://doi.org/10.3390/s18051437

Hsu, T.Y., Pham, Q.V., Chao, W.C. and Yang, T.S. (2020), "Post-earthquake building safety evaluation using consumer-grade surveillance cameras", *Smart Struct. Syst., Int. J.*, **25**(5), 531-541. https://doi.org/10.12989/sss.2020.25.5.531

Kim, J.M., Han, M., Lim, H.J., Yang, S. and Sohn, H. (2016a), "Operation of battery-less and wireless sensor using magnetic resonance based wireless power transfer through concrete", *Smart Struct. Syst., Int. J.*, **17**(4), 631-646. https://doi.org/10.12989/sss.2016.17.4.631

Kim, R.E., Li, J., Spencer, B.F., Nagayama, T. and Mechitov, K.A. (2016b), "Synchronized sensing for wireless monitoring of large structures", *Smart Struct. Syst., Int. J.*, **18**(5), 885-909. https://doi.org/10.12989/sss.2016.18.5.885

Kohler, M.D., Massari, A., Heaton, T.H., Kanamori, H., Hauksson, E., Guy, R., Clayton, R.W., Bunn, J. and Chandy, K.M. (2016), "Downtown Los Angeles 52-story high-rise and free-field response to an oil refinery explosion", *Earthq. Spectra*, **32**(3), 1793-820. https://doi.org/10.1193/062315EQS101M

Kong, Q., Allen, R.M. and Schreier, L. (2016a), "Myshake: Initial observations from a global smartphone seismic network", *Geophys. Res. Lett.*, **43**, 9588-9594. https://doi.org/10.1002/2016GL070955

Kong, Q., Allen, R.M., Schreier, L. and Kwon, Y.W. (2016b), "MyShake: A smartphone seismic network for earthquake early warning and beyond", *Sci. Adv.*, **2**(2), e1501055. https://doi.org/10.1126/sciadv.1501055

Kong, Q., Allen, R.M., Kohler, M.D., Heaton, T.H. and Bunn, J. (2018), "Structural health monitoring of buildings using smartphone sensors", *Seismol. Res. Lett.*, **89**, 594-602. https://doi.org/10.1785/0220170111

Lei, B., Ren, Y., Wang, N., Huo, L. and Song, G. (2020), "Design of a new low-cost unmanned aerial vehicle and vision-based concrete crack inspection method", *Struct. Health Monit.*, **19**(6), 1871-1883. https://doi.org/10.1177/1475921719898862

Mei, Q. and Gul, M. (2018), "A crowdsourcing-based methodology using smartphones for bridge health monitoring", *Struct. Health Monit.*, **18**(5-6),1602-1619. https://doi.org/10.1177/1475921718815457

Miškinis, R., Smirnov, D., Urba, E. and Dzindzelėta, B. (2011), "Timing and synchronization in mobile telecommunication networks. Frequency Control and the European Frequency and Time Forum (FCS)", *Proceedings of 2011 Joint Conference of the IEEE International*, San Francisco, CA, USA, May, pp. 665-669.

Naeim, F., Hagie, S., Alimoradi, A. and Miranda, E. (2006), "Automated post-earthquake damage assessment of instrumented buildings", In: *Wasti ST*, *Ozcebe G.* (*eds.*) *Advances in Earthquake Engineering for Urban Risk Reduction. Nato Science Series*: *IV*: *Earth and Environmental Sciences*, vol 66. Springer, Dordrecht, Netherlands.

Ozer, E., Feng, M.Q. and Feng, D. (2015), "Citizen sensors for SHM: Towards a crowdsourcing platform", *Sensors*, **15**, 14591-14614. https://doi.org/10.3390/s150614591

Shen, Y., Fu, W., Luo, Y., Yun, C.B., Liu, D., Yang, P., Yang, G. and Zhou, G. (2021), "Implementation of SHM system for Hangzhou East Railway Station using a wireless sensor network", *Smart Struct. Syst., Int. J.*, **27**(1), 19-33. https://doi.org/10.12989/sss.2021.27.1.019

Shrestha, A., Dang, J. and Wang, X. (2018), "Development of a smart-device-based vibration measurement system: Effectiveness examination and application cases to existing structure", *Struct. Control Health Monit.*, **25**, e2120. https://doi.org/10.1002/stc.2120

Sun, Z., Krishnan, S., Hackmann, G., Yan, G., Dyke, S.J., Lu, C. and, Irfanoglu, A. (2015), "Damage detection on a full-scale highway sign structure with a distributed wireless sensor network", *Smart Struct. Syst., Int. J.*, **16**(1), 223-242. https://doi.org/10.12989/sss.2015.16.1.223

Sun, K., Zhang, W., Ding, H., Kim, R.E. and Spencer Jr, B.F. (2017), "Autonomous evaluation of ambient vibration of underground spaces induced by adjacent subway trains using high-sensitivity wireless smart sensors", *Smart Struct. Syst., Int. J.*, **19**(1), 1-10. https://doi.org/10.12989/sss.2017.19.1.001

Yu, Y., Han, R., Zhao, X., Mao, X., Hu, W., Jiao, D. and Ou, J. (2015), "Initial validation of mobile-structural health monitoring method using smartphones", *Int. J. Distrib. Sensor Networks*, 1871230. https://doi.org/10.1155/2015/274391

Yu, Q., Guan, B., Shang, T., Liu, X. and Li, Z. (2019), "Flexible camera series network for deformation measurement of large scale structures", *Smart Struct. Syst., Int. J.*, **24**(5), 587-595. https://doi.org/10.12989/sss.2019.24.5.587

Zonta, D., Wu, H., Pozzi M., Zanon, P., Ceriotti, M., Mottola, L., Picco, G.P., Murphy, A.L., Guna, S. and Corra, M. (2010), "Wireless sensor networks for permanent health monitoring of historic buildings", *Smart Struct. Syst., Int. J.*, **6**(5), 595-618. https://doi.org/10.12989/sss.2010.6.5_6.595

HJ